

# Digital Beamforming in Elevation for Moving Surface Ships

Lin Zhang and Yicheng Jiang\*

**Abstract**—Moving target ship imaging in large sea area has always been the focus of military and civilian attention. Due to the limitation of pulse repetition frequency (PRF), there is a contradiction between wide mapping band and azimuth accuracy. The nonlinearity of PRF can also cause discontinuity of mapping band. Therefore, this paper proposes a method of digital beamforming-scan on receiving (DBF-SCORE) beam scanning based on airborne phased array radar to achieve the requirement of scene mapping band with lower PRF. The adaptive Capon spectrum estimation is used to dynamically adjust the beam pointing so that it can always point to the moving target for accurate imaging. Considering the nonuniform sampling of the transmitting pulse period of the antenna, the azimuth nonuniform Fourier transform (NUDFT) algorithm is used to re-sample the nonuniform periodic signal of the multi-channel receiving antenna and obtain the uniform spectrum signal. Finally, fine focusing of moving target is achieved by local phase gradient algorithm (PGA) algorithm, and accurate imaging of moving target in large sea area is realized. The validity of the algorithm can be verified by simulation and real data imaging, which can be used for reference in phased array SAR imaging of moving targets.

## 1. INTRODUCTION

In the past few decades, phased-array radars based on electronically scanned nonmoving parts have been developed significantly. These radars were originally developed to track multiple maneuvering and fast targets (such as aircraft and missiles), and they have the advantages of unique beam flexibility, high resolution, and fast panoramic scanning, which make their performance superior to that of traditional single-channel radars. Therefore, in recent years, phased-array radars have been extensively used in multitarget tracking, wide-area high-resolution scene surveying, and regional extreme climate monitoring and short-term forecasting [1]. The ocean continues to become increasingly more important in military and civilian fields, and therefore, as the next generation of surveillance radars, phased-array radars are playing an important role in sea surface imaging and moving-target detection.

For a traditional single-channel synthetic aperture radar (SAR), a large antenna beamwidth is required to achieve a large range of transmission and reception. Because the beamwidth is inversely proportional to the size of the antenna aperture, a smaller antenna size is consequently necessary for wide-swath imaging. However, because a single-channel SAR is restricted by the minimal antenna area, the antenna gain decreases with decreasing antenna size, which results in a substantial degradation in the imaging performance of the radar. In addition, wide beam in the elevation also causes blurring in the range direction of the image domain. Therefore, to achieve high resolution in the azimuth direction and wide-range swaths in the range direction spontaneously, lower transmission pulse repetition frequency (PRF) and multiple channels for echo receiving are required to resolve the contradiction between the two. This model demonstrates the formation of a multiphase center in the azimuth direction [2], which has been verified by the novel multifrequency polarized airborne SAR [3] of the German Aerospace Center (DLR) and Canadian second commercial Earth observation SAR satellite [4]; its major problems are channel calibration and azimuth signal reconstruction.

---

*Received 12 April 2019, Accepted 27 June 2019, Scheduled 26 July 2019*

\* Corresponding author: Yicheng Jiang (jiangyc@hit.edu.cn).

The authors are with the School of Electronics and Information Engineering, Harbin Institute of Technology, Harbin 150001, P. R. China.

Based on the azimuth multiphase center model, digital beamforming (DBF) has been developed and gradually become essential. DBF splits the original receiving antenna into multiple channels connected to separate receiving channels. The DBF development project was initiated by the German DLR in 2014. Based on this multiple-receiving-channel model, the project uses transmission beams with large elevation angles for illumination and narrow receiving beams to scan and track the pulse echoes on the ground — also referred to as the ScanSAR imaging mechanism — which enables SAR imaging with a meter-level resolution in a 200–250-km band [5]. The DBF system can control the pointing direction of multiple antenna subbeams at the receiving end through phase weighting, thereby integrating clutter suppression, beam scanning, and high-gain narrow-beam accurate imaging, which solves the traditional phased-array radar’s disadvantages of not being able to control beam direction because of fixed channel size.

Although DBF has been applied to actual airborne SAR systems, studies on its use in the accurate imaging of moving targets in a large scene remain inadequate. On the basis of previous studies, this study reconstructs the moving target imaging scene. In terms of elevation imaging, the DBF-SCORE algorithm was utilized, and the degree of arrival (DOA) of the moving target’s signal source in the elevation direction was accurately estimated by the adaptive Capon spectrum. Subsequently, the beam direction was adjusted so that the receiving beam would accurately point to the source position at any time, and the echo from the moving target was compressed into a finite resolution cell to facilitate the collection of the echo from the moving target. In terms of azimuth signal reconstruction, nonuniform discrete Fourier transform (NUDFT) was adopted to resample the nonuniform signals received by multiple antennas and convert them into uniform signals in the frequency domain spectrum, thereby effectively restoring the support area of the spectrum and achieving high-resolution imaging in the Doppler domain. Finally, the Doppler frequency parameters were estimated by a time-frequency analysis algorithm to complete the azimuth offset correction and coarse focus of the moving target, whereas the fine focus of the local moving target was achieved by the phase gradient autofocus (PGA) algorithm, thereby realizing the accurate imaging of moving targets in a large-scene sea area. Compared with the traditional DBF algorithm, the proposed algorithm has significantly enhanced imaging performance and solves the problem of imaging blurring for moving targets.

## 2. ELEVATION DBF SIGNAL MODEL

The elevation DBF model is shown in Fig. 1. It uses a single-transmitting multireceiving mode. The transmission end is composed of a transmitting antenna utilizing a full-aperture wide beam. The

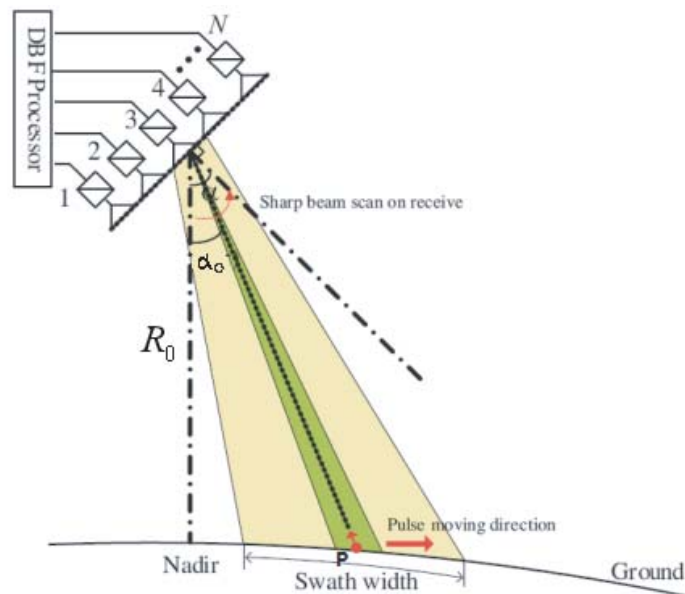


**Figure 1.** Schematic of the elevation DBF imaging model.

receiving end is composed of  $N$  subantennas equally spaced  $d$  in the azimuth direction. Each antenna acquires samples independently, and all subantennas receive the echoes simultaneously, performing DBF in the elevation direction.

The instantaneous distance between the moving target  $P$  and the transmitting antenna is:

$$R_1 = \sqrt{(R_0 + V_r t_m)^2 + (V t_m - V_a t_m)^2} \approx R_0 + V_r t_m + \frac{(V_r^2 + (V - V_a)^2)}{2R_0} t_m^2 \quad (1)$$

Here,  $R_0$  is the vertical distance from the aircraft to the target.  $V_a$  is the along-track velocity of the target point  $P$ , and  $V_r$  is the radial velocity of  $P$ , which is positive away from the track.  $V$  is the flight velocity of the carrier.

The instantaneous distance between the moving target  $P$  and the  $n$ th receiving antenna is:

$$R_k = \sqrt{(R_0 + V_r t_m)^2 + (V t_m - V_a t_m - d_n)^2} \approx R_0 + V_r t_m + \frac{(V_r^2 + (V - V_a)^2)}{2R_0} t_m^2 + d_n \cdot \sin(\alpha(t) - \alpha_0) \quad (2)$$

where  $\alpha_0$  is the view angle of target, also referred to as beam view angle. At  $\alpha_0$ , the beam points directly to the target point  $P$ , resulting in the largest antenna gain.  $\alpha(t)$  is the antenna's normal angle, which changes with the beam direction. When the beam is not pointed toward the center of the azimuth imaging area,  $\alpha(t)$  is less than  $\alpha_0$ , and, therefore, the beam's echo delay is smaller than the reference time  $\tau_0$ , whose difference is the delay difference caused by the beam view angle in the range direction. On the contrary, when the beam sweeps through the center of the azimuth imaging area,  $\alpha(t)$  is greater than  $\alpha_0$ ; therefore, the beam's echo delay is larger than the reference time  $\tau_0$ .

Therefore, the delay of the transmitted signal from the transmitting channel to the target and then reflected to the  $n$ th receiving beam is:

$$\tau_n = \tau_0 - \frac{d_n \cdot \sin(\alpha_0 - \alpha(t))}{c} \quad (3)$$

where  $\tau_0$  is the return time from the phase center of the transmitting antenna to the target, and  $d_n$  denotes the distance between the  $n$ th receiving channel and the reference channel;  $d_n = (N - 1) \cdot d$ .

The echo signal received by each channel in the range direction is:

$$s_n(\tau) = \gamma \cdot \text{rect} \left[ \frac{\tau - \tau_n}{T_p} \right] \cdot \exp(-j2\pi \cdot f_c \cdot \tau_n) \cdot \exp \left[ jk_r \pi (\tau - \tau_n)^2 \right] \quad n = 1, 2, \dots, N \quad (4)$$

where  $\gamma$  is a constant related to the target scattering coefficient and the antenna pattern gain,  $f_c$  the radar's carrier frequency,  $k_r$  the frequency modulation rate, and  $T_p$  the pulse width. After each channel is down-converted, the received echo signal is transformed to:

$$\begin{aligned} s_n(\tau) &= \gamma \cdot \text{rect} \left[ \frac{\tau - \tau_n}{T_p} \right] \cdot \exp(-j2\pi \cdot f_c \cdot \tau_n) \cdot \exp \left[ jk_r \pi (\tau - \tau_n)^2 \right] \\ &= \gamma \cdot \text{rect} \left[ \frac{\tau - \tau_n}{T_p} \right] \cdot \exp \left[ jk_r \pi (\tau - \tau_n)^2 \right] \cdot \exp(-j2\pi f_c \tau_0) \cdot \exp(-j2\pi \cdot d_n \cdot \sin(\alpha(t) - \alpha_0)/\lambda) \\ & \quad n = 1, 2, \dots, N \end{aligned} \quad (5)$$

Therefore, the steering vector  $a(\alpha_0)$  of the elevation signal received by multiple antennas is:

$$\begin{aligned} a(\alpha_0) &= \left[ 1, \exp \left( -j \frac{2\pi}{\lambda} d \cdot \sin(\alpha - \alpha_0) \right), \exp \left( -j \frac{2\pi}{\lambda} 2d \cdot \sin(\alpha - \alpha_0) \right), \right. \\ & \quad \left. \exp \left( -j \frac{2\pi}{\lambda} (N - 1) d \cdot \sin(\alpha - \alpha_0) \right) \right] \end{aligned} \quad (6)$$

According to the classical beamforming theory [6], to register the echoes received by each antenna and adjust the beam directions to focus on one point, the weighting coefficient of each channel should be:

$$w_n(t) = \exp(j2\pi \cdot d_n \cdot \sin(\alpha - \alpha_0)/\lambda) \quad (7)$$

Consequently, after being processed by compression in the range direction and DBF weighting, the result of the beamforming is:

$$y(\tau) = \sum_{n=1}^N s_n(\tau) \cdot w_n(\tau) = \frac{\sin [N\pi d(\sin(\alpha - \alpha_0))/\lambda]}{\sin [\pi d(\sin(\alpha - \alpha_0))/\lambda]} \cdot \sin c [k_r T_p (\tau - \tau_0)] \quad (8)$$

The above procedures realize the DBF of moving targets. The key of DBF is that it utilizes the approximate linear relationship between the normal offset angle  $\alpha(t)$  of the target and its corresponding elevation echo time, which is equivalent to the approximate linear relationship between the target elevation angle and its range gate. The strong echo information of the target determines the phase rotation angle that each subantenna needs to adjust, and once each receiving channel is changed by the corresponding angle via weighting, the centers of all beams point to the target scene, thereby realizing the tracking of the moving target by narrow digital beams, which prolongs the synthetic aperture time of the moving target, escalates the receiving gain, and facilitates the accurate imaging of the moving target.

### 3. ADAPTIVE CAPON SPECTRAL ESTIMATION

The DBF model is critical for phased-array radars to resolve the problem of moving ship imaging in large sea areas. As the Capon spectral estimation provides high accuracy for estimating the source direction of a moving target, it is particularly useful for real-time tracking and positioning of ships. Therefore, the Capon spectral estimation was adopted to analyze the echo signals of surface ships and acquire the elevation beam direction, thereby completing the adaptive DBF process in the range direction.

The Capon beamformer was first proposed by Capon in 1969 [7], when he called it “minimum variance distortionless response” (MVDR) beamformer. MVDR uses part of the degree of freedom to form the main beam in the user’s expected direction and, in the meantime, utilizes the remaining degree of freedom to create a zero point in the direction of the interference signal. As a result, it can keep the power contributed by interferences from any directions other than the source direction, such as noises, to a minimum, while maintaining the signal power in the source direction. The working principle of Capon spectral estimation makes it possible to approximate it as a sharp spatial bandpass filter, which requires the weight vector  $w$  to satisfy two conditions.

$$(1) \text{ To form the beam: } w^H \cdot a(\theta_d) = a^H(\theta_d) \cdot w = 1 \quad (9)$$

$$(2) \text{ To form the zero point: } w^H \cdot a(\theta_n) = a^H(\theta_n) \cdot w = 0 \quad (10)$$

Here,  $\theta_d$  is the direction of the target’s source signal, and  $\theta_n$  is the direction of the interference. By searching for each angular degree of freedom that can be utilized, the received energy is focused in the direction where the target is located. The optimization of the constraint condition (1) guarantees the correct reception of the expected signal, and constraint condition (2) implies the suppression of noises in other directions, especially where sea clutters can be generated.

Capon spectral estimation first utilizes part of the training samples acquired in the azimuth direction to estimate the location of the source, which obtains an accurate angle corresponding to each source within the range gate. Then, according to the angle, the weight vector and beam direction of each range gate are adjusted periodically, so that the subsequent echoes are consistently received with a high gain, and the motion status of the moving target is closely tracked. The Capon spectral estimation increases the signal-to-noise ratio of the system and solves the limited duration of moving target imaging when sea clutters are large.

Prior to performing Capon spectral estimation, the received signal is compressed in the range direction. By compressing the source’s diffused energy in the time domain to its corresponding range gate, the estimation accuracy in the source direction can be improved. Compressing Equation (5) gives:

$$y_{rc}(\tau) = \gamma \cdot \sin c [k_r T_p (\tau - \tau_0)] \cdot \exp(-j2\pi f_c \tau_0) \cdot \exp \left[ -j \frac{2\pi}{\lambda} d_n \cdot \sin(\alpha(t) - \alpha_0) \right] \\ \cdot \text{rect} \left( \frac{t - t_0}{T_{sar}} \right) \cdot \exp \left( -j \frac{2\pi}{\lambda} (R_1 + R_k) \right) \quad (11)$$

After range compression is completed, maximum-likelihood estimation is conducted on the signal covariance matrix of each range gate, whose expression is:

$$\hat{R}_y(\tau) = \frac{1}{N} \sum_{n=1}^N y_{rc}(\tau, n) \cdot y_{rc}^H(\tau, n) = E [y_{rc}(\tau, n) \cdot y_{rc}^H(\tau, n)] = a(\theta)R_{xx}a^H(\theta) + \sigma_n^2 I, \quad (12)$$

where  $E[\cdot]$  denotes the statistical mean,  $R_{xx} = E[y_{rc}(t) \cdot y_{rc}^H(t)]$  the covariance matrix of the signal (which is a nonsingular matrix when the target source is noncoherent),  $\sigma_n$  the noise power, and  $I$  the identity matrix of  $Nr$ .

The Capon spectral estimation obtains the optimal weight vector that maximizes the target's signal-to-noise ratio by minimizing the output energy of the matrix, i.e., minimizing the contribution of the interference. This requires:

$$\min_w E [ |y_{rc}(t)|^2 ] = \min_w E \{ w^H R_{xx} w \} \quad (13)$$

The weight vector  $w$  can be solved by applying Lagrange multiplication, and the objective function can be established by:

$$L(w) = w^H R_{xx} w + \lambda [1 - w^H a(\theta_d)] \quad (14)$$

If one defines  $\frac{\partial L(w)}{\partial w} = 0$ , then  $R_{xx} w - \lambda a(\theta_d) = 0$ , and consequently:

$$w_{opt} = \lambda R_{xx}^{-1} a(\theta_d) \quad (15)$$

Because  $w^H \cdot a(\theta_d) = 1$ , one has:

$$\lambda = \frac{1}{a^H(\theta_d) R_{xx}^{-1} a(\theta_d)} \quad (16)$$

Therefore, the optimal weight vector is:

$$w_{opt} = \frac{R_{xx}^{-1} a(\theta_d)}{a^H(\theta_d) R_{xx}^{-1} a(\theta_d)} \quad (17)$$

Consequently, the power of the Capon spatial spectrum is:

$$P(\theta) = \min_w E \{ w^H R_{xx} w \} = w_{opt}^H \cdot R_{xx} \cdot w_{opt} = \frac{a^H(\theta_d) \cdot (R_{xx}^{-1})^H \cdot R_{xx} \cdot w_{opt}}{a^H(\theta) \cdot R_{xx}^{-1} \cdot a(\theta)} = \frac{1}{a^H(\theta) \cdot R_{xx}^{-1} \cdot a(\theta)} \quad (18)$$

By finding the peak position in the spatial spectrum  $P(t, \theta)$ , the source DOA value corresponding to time  $t$  can be derived. The estimated  $\hat{\theta}_0$  can be used to derive the weighting coefficient  $w(t)_{opt} = \frac{R_{xx}^{-1} \cdot a(\theta_0)}{a^H(\theta_0) R_{xx}^{-1} a(\theta_0)}$  of each range gate, which can be adopted to adjust the beam of the gate corresponding to each channel, thereby further improving the resolution of elevation imaging.

#### 4. AZIMUTH NONUNIFORM PRF SAMPLE RECONSTRUCTION

Multichannel signals use low PRF sampling to realize large-scene imaging in the azimuth direction. It is known from beam position design that different PRFs correspond to different swath widths. Therefore, the PRF must be variable to cover the swaths continuously. If the PRF does not satisfy uniform sampling, the azimuth signal is acquired nonuniformly, and additionally, pairwise false targets are formed on both sides of the main waveform [8]. In processing the multichannel nonuniform signals, the azimuth nonuniform PRF samples are converted using the NUDFT algorithm to complete uniform sample reconstruction. NUDFT can realize the bidirectional conversion of input nonuniform data to output uniform data in any domain (time or frequency domain). Compared with the traditional reconstruction process that adopts the sinc function to interpolate one-dimensional data, NUDFT has the advantages of higher accuracy and faster calculations. In the NUDFT algorithm, Dutt and Rokhlin [9] were the first to use the kernel function of the Gaussian clock to calculate the interpolation coefficients, followed by Fessler and Sutton [10] using the min-max method to calculate the interpolation coefficient of each frequency point, through which the minimal worst error value can be derived. Subsequently, Liu and

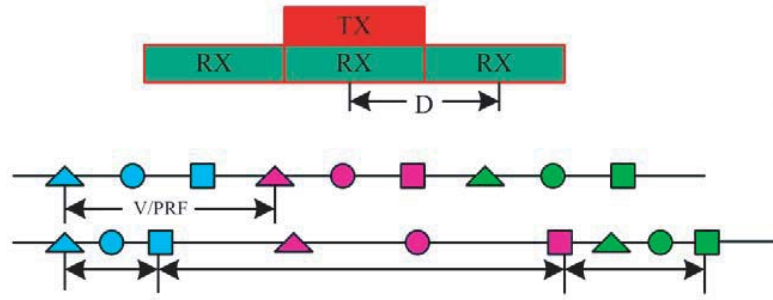


**Figure 2.** Schematic of uniform and nonuniform sampling in the azimuth direction.

Nguyen [11] proposed a sparse constraint least-squares inversion method based on Fourier transform. All these methods essentially use polynomials to perform highly accurate fitting of the data  $e^{it_k \cdot w_j}$ , so that the corresponding frequency domain components of the nonuniform samples in the time domain can be obtained via NUDFT. When NUDFT is applied to the azimuth processing of SAR imaging [12, 13], the deviation of PRF from the optimal sampling frequency causes the period of the echo signal's PRF to be nonuniform. For multichannel received signals, it instead exhibits a periodic nonuniform sampling characteristic, as shown in Fig. 2.

For a nonuniformly distributed sampling sequence  $t_n$ ,  $t_n \in [-\frac{Na}{2}, \frac{Na}{2} - 1]$ . Because  $t_n$  is the time vector of the azimuth nonuniform samples, the discrete Fourier transform of the data signal  $f(t_n)$  at point  $N_a$  is:

$$f_j = \sum_{n=-Na/2}^{Na/2-1} a_k \cdot e^{it_n w_j}, \quad (19)$$

where  $w_j = \frac{2\pi j}{Na}$ ,  $j = -\frac{Na}{2} \dots \frac{Na}{2} - 1$ ,  $n = -\frac{Na}{2} \dots \frac{Na}{2} - 1$ ,  $a_k$  is the echo signal of the azimuth nonuniform samples of the variable PRF, and  $f_j$  is the uniform frequency domain component of the output.

The echo signals are first transformed into uniform frequency domain line-by-line in the azimuth direction using the NUDFT algorithm. Subsequent imaging is completed via the estimation of the Doppler parameter of the moving target and the adoption of conventional frequency domain imaging algorithms. However, because the receiving angles of the subantennas are different, there are phase differences as a result of changes in the antenna viewing angle in the respective imaging processes. Especially for a moving target, during the aperture synthesis of imaging, the dynamic rotation angle of the receiving antenna incurs an accumulated phase error in phase compensation. Therefore, the local PGA algorithm is required to allow the autofocus of images in the azimuth direction for fuzzy regions, because it not only ensures the scene space of the imaging area, but also achieves accurate imaging of moving targets.

## 5. LOCAL PGA ALGORITHM

The change in the antenna view angle and the swing of a moving ship both introduce phase errors. Although Doppler estimation can realize the coarse compensation of phase error, to improve the accuracy of the low-frequency component compensation of phase error, this study further adopts the local PGA algorithm to achieve the fine phase compensation of moving surface ships. The approximation of the phase error by the PGA algorithm is accomplished by multiple iterations between the complex image and the Doppler phase history. Because each iteration requires Fourier transform, the amount of calculation is substantial. In this work, under the phased-array scenario, the beam direction is instead combined with the PGA algorithm. Because the beam direction of the antenna array already determined the range DOA, the step of selecting the range line in the traditional PGA algorithm was saved at the cost of limiting the applicable scenario of the PGA algorithm to the finite range line where the target ship was located. However, one of the prerequisites of the PGA algorithm is that the point target on the selected range line is isolated [14], that is, if there are multiple scattering points on the range line

that are close to each other, their reflection areas are coupled, affecting the accuracy of phase error estimation. Therefore, when one estimates the phase error of a ship, whether there are other ships close to the target ship must be clarified. Alternatively, the selected window size can be adjusted to only include the target ship, and therefore, its error support area is not influenced by other ships.

Although the sea area is vast, because this study only focused on the fine imaging of a moving ship, the original segmented PGA algorithm for large scenes [15] was replaced with the local PGA algorithm — that is, first the range line where the ship was located was identified, and then the PGA algorithm was adopted to apply cyclic shift, window selection, phase gradient estimation, phase error correction, and iteration to the target ship so as to complete the entire phase error correction process of the individual ship. Because the range and azimuth cells of the ship were relatively small, the nonemptiness of the phase in the range and the azimuth direction were ignored. However, in the process of completing the image stitching for each ship, the linear translation of the image must be considered, which can be achieved by using the subimage correlation method. The implementation of the local PGA algorithm not only reduces the number of iterations, but also improves the accuracy of phase error estimation. In summary, the flowchart of imaging moving surface ships is shown in Fig. 3.

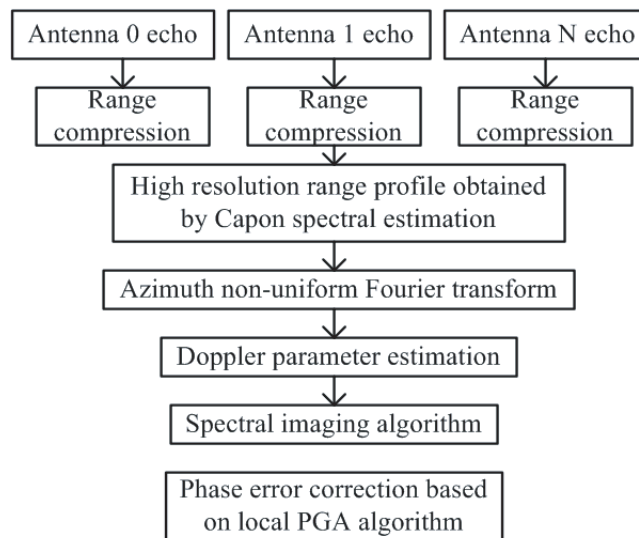


**Figure 3.** Flow chart of imaging moving surface ships.

## 6. SIMULATION AND MEASURED DATA ANALYSIS

In this study, an elevation DBF imaging model for sea surface phased-array radars is established for the simulation verification of surface ships. The simulation parameters are listed in Table 1. The simulation scene assigns a moving point to represent a ship and uses the Capon algorithm to calculate the optimal weight vector of each receiving antenna, so that the overall receiving beam can accurately point to the

**Table 1.** Surface ship simulation parameters.

Carrier frequency (GHz)	1.5	Transmitter pulse duration ( $\mu\text{s}$ )	1.5
Slant range (km)	3	Transmitter pulse bandwidth (MHz)	150
Carrier velocity (m/s)	200	A/D sampling rate (MHz)	256
Number of phased-array antennas	32	Ship initial coordinates ( $X, Y$ )	(10, 50)
Antenna spacing (m)	2	Ship radial velocity ( $V_r$ ) (m/s)	5
PRF (Hz)	384	Ship along velocity ( $V_a$ ) (m/s)	20

source position at any time, as shown in Figs. 4(a) and 4(b).

Figure 4(a) shows the fixed beam directions of each receiving antenna with a stationary target, which are  $-20^\circ$ ,  $0^\circ$ , and  $30^\circ$ . The signal covariance matrix of each range gate is calculated by the Capon algorithm, which is subsequently used to derive the elevation spatial spectral power via Equation (18). Upon finding the peak position in the spatial spectral power curve, the DOA value of the source stationary target is derived. Fig. 4(b) demonstrates the continuous curve of beam direction for a moving target with a radial velocity alone or both a radial velocity and a radial acceleration. This curve indicates that the beam direction changes with the motion of the moving target; therefore, it always illuminates the moving target point, thereby increasing the duration of aperture synthesis. Fig. 5 compares the resolutions in the range direction of multichannel and single-channel beamforming systems. The multichannel system is composed of 32 subantennas, whose overall beam direction is

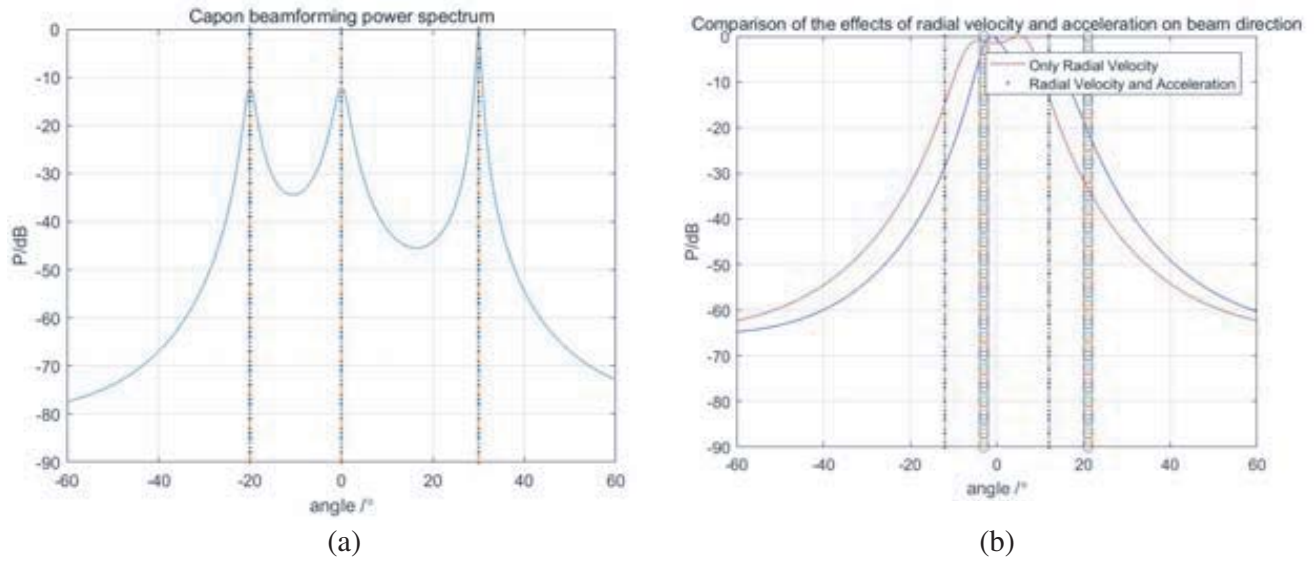


**Figure 4.** (a) Spatial spectral power of the Capon algorithm for a stationary point target. (b) Comparison of the effects of radial velocity and radial acceleration of the point target on the beam direction.

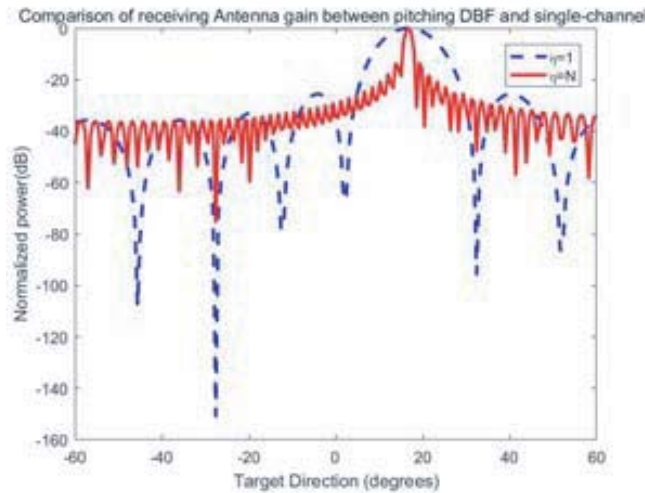
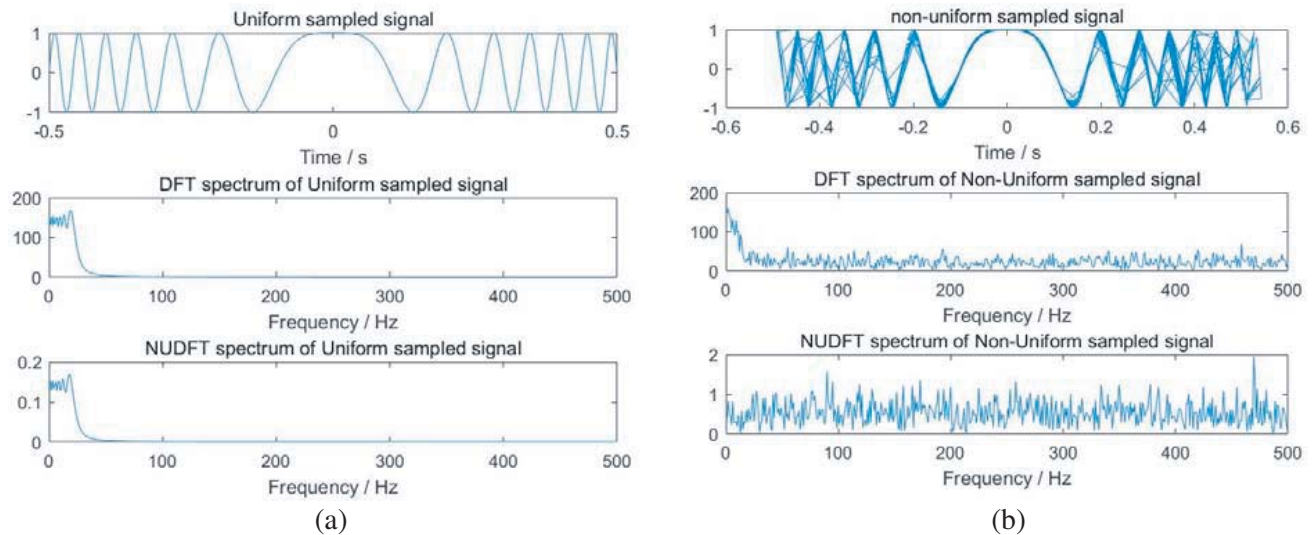


**Figure 5.** Comparison of the resolutions in the range direction of multichannel and single-channel beamforming systems.

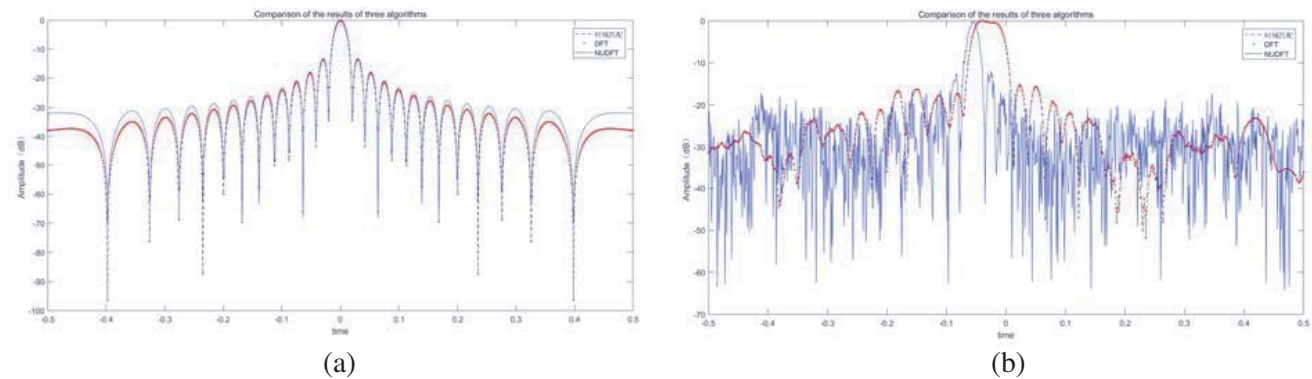
approximately  $20^\circ$ . Its resolution in the range direction is 32 times that of the single-channel system, which is proportional to the number of antennas in the multichannel system.

Figure 6 shows the azimuth discrete spectra processed by the DFT and NUFT algorithms of uniformly sampled and nonuniformly sampled signals. Fig. 6 shows that for uniformly sampled signals, the discrete spectra processed by the DFT and NUFT algorithms are similar, but for nonuniformly sampled signals, the NUFT algorithm obtains more transient spectral components according to the nonuniformity of the time domain, thereby demonstrating a finer spectral expression. Fig. 7 compares three imaging methods for a point target, which suggests that although DFT and NUFT present a similar imaging performance of azimuth uniformly sampled point targets, for nonuniform point targets, NUFT has narrower main lobe width and higher target resolution, which can suppress the generation of false targets on both sides of the main lobe.

On the basis of point target simulation verification of the algorithm, this study further uses the measured data of a certain sea area in China to image surface ships. Because ships swing when moving or in a windy environment, as traditional SAR imaging techniques are utilized, low-order phase errors always exist, even if Doppler parameter estimation and compensation are performed for the inertial navigation coefficient, causing the image of the moving ship to be blurred, as shown in Fig. 8. The traditional PGA algorithm uses the maximum energy method to select the range line and uses the



**Figure 6.** (a) DFT spectrum and NUFT spectrum of uniformly sampled signals. (b) DFT spectrum and NUFT spectrum of nonuniformly sampled signals.



**Figure 7.** (a) Comparison of uniformly sampled signal point targets. (b) Comparison of nonuniformly sampled signal point targets.

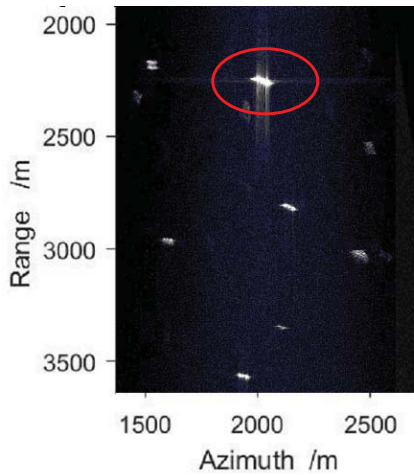


**Figure 8.** Conventional SAR imaging.

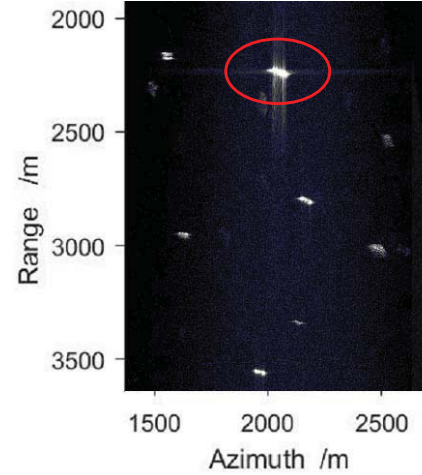


**Figure 9.** Traditional PGA imaging.

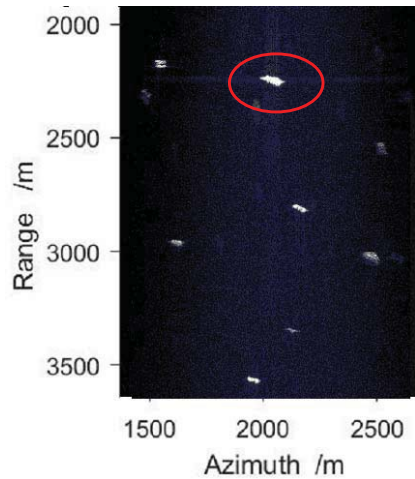


**Figure 10.** Local PGA imaging.

window to fix the length. Although the azimuth phase error is corrected to some extent, it is still unable to focus each ship adaptively. As shown in Fig. 9, the image of moving ship A is blurred. This is due to the dislocation of one-dimensional distances between warships in the course of shaking. The traditional PGA algorithm neglects the spatiality in the range direction and can only solve the phase error in the azimuth direction, so the imaging effect cannot achieve the function of self-focusing. The local PGA algorithm proposed in this paper can focus the target separately in the range unit, which is helpful for iterative processing and window suppression of clutter for each moving ship, so that all moving ships can achieve self-focusing state and improve the imaging accuracy of ships in wide sea area, as shown in Fig. 10.

## 7. CONCLUSION

This study utilizes the phased-array DBF algorithm for dynamically monitoring and accurately imaging moving surface ships. The following conclusions are drawn. First, under a phased-array SAR scene, the DBF algorithm can consistently point the combined beam to the moving target, which helps compress the signal into the finite range gate to realize the scanning imaging of a wide scene. Second, the NUDFT algorithm can resolve the echo reconstruction of nonuniform samples, which overcomes the strict limitations of traditional imaging on PRF. Last, the local PGA algorithm can compensate the

remaining fuzzy phases of ships and obtain more-accurate imaging information of moving targets. The simulation and measured data verification indicate that this algorithm presents good imaging performance of sea surface moving targets in a large scene, thereby demonstrating significant application values in future naval battles or civil marine monitoring.

## ACKNOWLEDGMENT

This work was supported by the National Natural Science Foundation of China for General Program under Grant No. 61671490; the National Key R&D Program of China under Grant No. 2016YFB0100901.

## REFERENCES

1. Heimner, J., "Multi-mission phased array radar (MPAR) national radar R&D project," *Systems, Applications & Technology Conference*, 1–2, IEEE Long Island, 2008.
2. Zhang, S. X., M. D. Xing, X. G. Xia, et al., "Multichannel HRWS SAR imaging based on range-variant channel calibration and multi-Doppler-direction restriction ambiguity suppression," *IEEE Transactions on Geoscience and Remote Sensing*, Vol. 52, No. 7, 4306–4327, 2014.
3. Reigber, A., A. Nottensteiner, M. Limbach, et al., "DBFSAR: An airborne very high-resolution digital beamforming SAR system," *Proceedings of the 14th European Radar Conference*, 175–178, Nuremberg, Germany, Oct. 2017.
4. Sikaneta, I. and D. Cerutti-Maori, "Demonstrations of HRWS and GMTI with RADARSAT-2," *European Conference on Synthetic Aperture Radar*, 263–266, Nuremberg, Germany, Apr. 2012.
5. Reigber, A., A. Nottensteiner, M. Limbach, et al., "DBFSAR: An airborne very high-resolution digital beamforming SAR system," *European Radar Conference (EuRAD)*, 175–178, 2017.
6. Cook, C. E. and M. Bernfeld. *Radar Signal an Introduction to Theory and Application*, Academic Press, 1967.
7. Capon, J., "High-resolution frequency-wavenumber spectral analysis," *Proc. IEEE*, Vol. 57, 1408–1418, 1969.
8. Zhang, C., *Synthetic Aperture Radar: Theory, System Analysis and Application*, Science Press, Beijing, 1989.
9. Dutt, A. and V. Rokhlin, "Fast Fourier transforms for nonequispaced data," *SIAM Journal on Scientific Computing*, Vol. 14, No. 6, 1368–1393, 1993.
10. Fessler, J. A. and B. P. Sutton, "Nonuniform fast Fourier transforms using min-max interpolation," *IEEE Transactions on Signal Processing*, Vol. 51, No. 2, 560–574, 2003.
11. Liu, Q. H. and N. Nguyen, "An accurate algorithm for nonuniform fast Fourier transforms (NUFFT's)," *IEEE Microwave and Guided Wave Letters*, Vol. 8, No. 1, 18–20, 2002.
12. Ren, B. L., S. Y. Li, H. J. Sun, et al., "A fast circular convolution algorithm based on NUFFT for near-field SAR imaging," *International Conference on Microwave & Millimeter Wave Technology*, 1–4, 2012.
13. Wu, Y., H. Song, X. Shang, et al., "Improved RMA based on Nonuniform Fast Fourier Transforms (NUFFT's)," *International Conference on Signal Processing*, 2489–2492, 2008.
14. Zhao, X., X. L. Wang, and Z. M. Wang, "Phase gradient autofocus algorithm for SAR images based on optimal contrast criterion," *Remote Sensing Technology and Application*, Vol. 20, No. 6, 606–610, 2005.
15. Ye, C., X. Ning, J. Yang, et al., "Parallel implementation of a block-wise phase gradient autofocusing method," *J. Tsinghua Univ. (Sci. & Tech.)*, Vol. 52, No. 5, 612–615, 2012.